IEEE Access
Multidisciplinary | Rapid Review | Open Access Journal

Received 11 March 2024, accepted 4 June 2024, date of publication 7 June 2024, date of current version 17 June 2024.

Digital Object Identifier 10.1109/ACCESS.2024.3411152

RESEARCH ARTICLE

Multi-Objective Optimization and Comparison of DC/DC Converters for Offshore Wind Turbines

VICTOR TIMMERS[1], AGUSTÍ EGEA-ÀLVAREZ[1], (Member, IEEE), ARIS GKOUNTARAS[2], AND LIE XU[1], (Senior Member, IEEE)

[1]Department of Electronic and Electrical Engineering, University of Strathclyde, G1 1XQ Glasgow, U.K.
[2]Siemens Gamesa Renewable Energy, 20097 Hamburg, Germany

Corresponding author: Victor Timmers (victor.timmers@strath.ac.uk)

This work was supported in part by the UK Engineering and Physical Sciences Research Council (EPSRC) under Industrial Cooperative Award in Science and Engineering (ICASE) under Grant EP/T517665/1, and in part by Siemens Gamesa Renewable Energy.

ABSTRACT A key enabling technology for DC collection systems in offshore wind farms is a suitable wind turbine DC/DC converter. However, there is no consensus regarding the topology, design, or operating frequency of this converter. This paper presents an optimization and comparison of four DC/DC converter topologies, including 1-phase, 3-phase, unidirectional, and bidirectional converters. The converters are compared in terms of their reliability, volume, weight and losses at switching frequencies ranging from 500 Hz to 5 kHz. The medium frequency transformer for each converter is designed using multi-objective optimization, and the overall converter volume calculation takes into account the insulation requirements and physical configuration of the components. The results show that if only unidirectional operation is required, the 1-phase single active bridge is the preferred option due to its high reliability, small size and low losses with an optimal operating frequency of up to 2.5 kHz. For bidirectional systems, the 1-phase and 3-phase dual active bridge topologies have a similar efficiency and optimal operating frequency of 1 kHz. Despite its higher volume, the 3-phase version is the preferred option due to its higher reliability and lower device stresses, provided there is enough available space.

INDEX TERMS DC-DC converter, design optimization, dielectrics and electrical insulation, Pareto optimization, reliability, wind energy.

I. INTRODUCTION

The offshore wind industry is expected to grow rapidly as the world aims to reduce its dependence on fossil fuels, with some estimates predicting 2000 GW of installed capacity by 2050, compared to just 35 GW in 2020 [1]. Offshore wind power plants and individual wind turbines have become increasingly large to benefit from economies of scale. For example, the European Grid operator TenneT is developing a standardized offshore wind platform with a capacity of 2 GW [2], and the latest generation of wind turbines have individual capacities of 15 MW [3]. At the same time, wind power plants are located increasingly far from shore as suitable near-shore locations are exhausted, and optimal wind resource is typically found in remote locations. Hence, the use of HVDC connections is expected to become commonplace in the next generation of wind farms.

Wind farms traditionally use medium voltage AC (MVAC) cables in their collection system, which means AC/DC converters are required to achieve HVDC power transmission. This is illustrated in Fig. 1a. The offshore platform houses this converter and its associated transformers, which together form one of the largest costs of the offshore wind power plant, accounting for 15–25% of the total capital cost [4]. In addition, the increasingly high power ratings of individual turbines results in higher cable losses and a reduction in the number of wind turbines per string, increasing cable costs.

These issues have generated significant interest in the use of medium voltage DC (MVDC) in the collection system instead of MVAC [5]. The resulting all-DC wind farm topology is illustrated in Fig. 1b. In this wind farm design, voltage transformation in the wind turbine and offshore substation is performed using DC/DC converters, which

The associate editor coordinating the review of this manuscript and approving it for publication was Sonia F. Pinto.

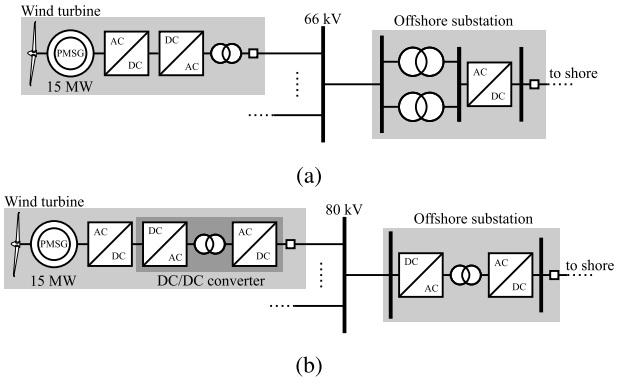

FIGURE 1. Offshore wind farm configurations, (a) traditional AC collection system with HVDC export system, (b) proposed all-DC wind farm with DC collection and export systems.

use medium frequency transformers (MFTs), leading to space and weight savings compared to conventional 50 Hz transformers.

The potential benefits of using DC collection systems are highly dependent on the design of the DC/DC converter [4], [6]. The selected converter topology and operating frequency will influence the size, efficiency and reliability of the system and therefore play a large role in the overall cost-effectiveness. This research focuses on the design and comparison of four wind turbine DC/DC converter candidates, expanding on previous multi-objective design optimization work by the authors [7], [8].

A. STATE OF THE ART

A significant number of DC/DC converter designs have been put forward in the literature, including isolated designs that use a medium frequency transformer (MFT) [9], [10], [11] and non-isolated designs that use resonance to increase the voltage [12], [13], [14]. Only isolated designs are considered in this paper, as they are preferred for safety considerations and have the additional benefit of facilitating the large voltage increase required between the wind turbine generator and collection system.

A number of publications have attempted to compare isolated DC/DC converter designs for wind turbine applications. In [15], the characteristics of six 6 MW, 2.8/100 kV converter topologies were compared, including non-resonant and resonant topologies. The assessment covered the component stresses, component count and losses. However, the study was limited since it assumed a single converter operating frequency and did not include any dimensional or reliability analysis of the converters.

A study by [16] investigated the power loss, volume and weight of six isolated 10 MW converter topologies, including three matrix-based converters and three back-to-back converters. They also investigated the impact of the MFT frequency and number of parallel connected modules. Their results show that the reduced matrix converter (RMC) had the highest efficiency over the whole frequency range, and low volume at frequencies above 7 kHz. The 1-phase and 3-phase full bridge converters were the next most efficient with comparable volumes at frequencies up to 3 kHz. However, matrix converters are unlikely to be commercially available in the near future due to their relatively high control complexity and lack of practical applications. The study also does not include any assessment of the reliability or insulation requirements.

In [17], the 1-phase dual active bridge (DAB1) and 3-phase dual active bridge (DAB3) were compared in terms of losses, volume and weight for a 10 MW, 1/50 kV converter. The converter consisted of 50 modules, each with a 1:1 transformer ratio. They found that the DAB1 and DAB3 have similar losses of around 1.5%, with the DAB3 having approximately 20% lower volume and weight. However, the study considered only bidirectional converters operating with a single frequency and did not assess the converter reliability or insulation.

B. CONTRIBUTIONS

This research provides the first comprehensive DC/DC converter optimization and comparison for DC-connected offshore wind turbines. The study is comprehensive as it covers multiple aspects of converter design, including the reliability, dielectric insulation, volume, weight, and losses for varying operating frequencies. The study includes a multi-objective optimization of the MFT and a volume optimization considering the insulation requirements. The DC/DC converter topologies included in the study include both 1-phase and 3-phase, unidirectional and bidirectional DC/DC converters.

Existing research only considers a limited number of these factors. For example, most studies consider a single DC/DC converter topology, which can be unidirectional or bidirectional. Proponents of the unidirectional converters argue that these provide the most cost-effective solution since wind turbines only need to deliver power. However, bidirectional power converters would allow for self-start capabilities in case of a black start, since power is required to energize the DC bus and to supply the auxiliary equipment [18]. The fault ride-through ability of unidirectional and bidirectional converters may also differ due to their differing degree of controllability. There is a lack of studies investigating how these two topology designs compare to each other.

This research is particularly relevant for offshore wind applications by being the first to include a dedicated reliability study. Reliability is a key factor due to the difficulty in accessing offshore equipment. In addition, the reliability calculations have knock-on effects for the rest of the converter design. For example, the desired reliability will influence the converter redundancy requirements, which in turn affects component stresses, which influence transformer design, which impacts the size and efficiency of the converter. This interplay of factors is frequently overlooked in existing comparison studies, especially where reliability is concerned.

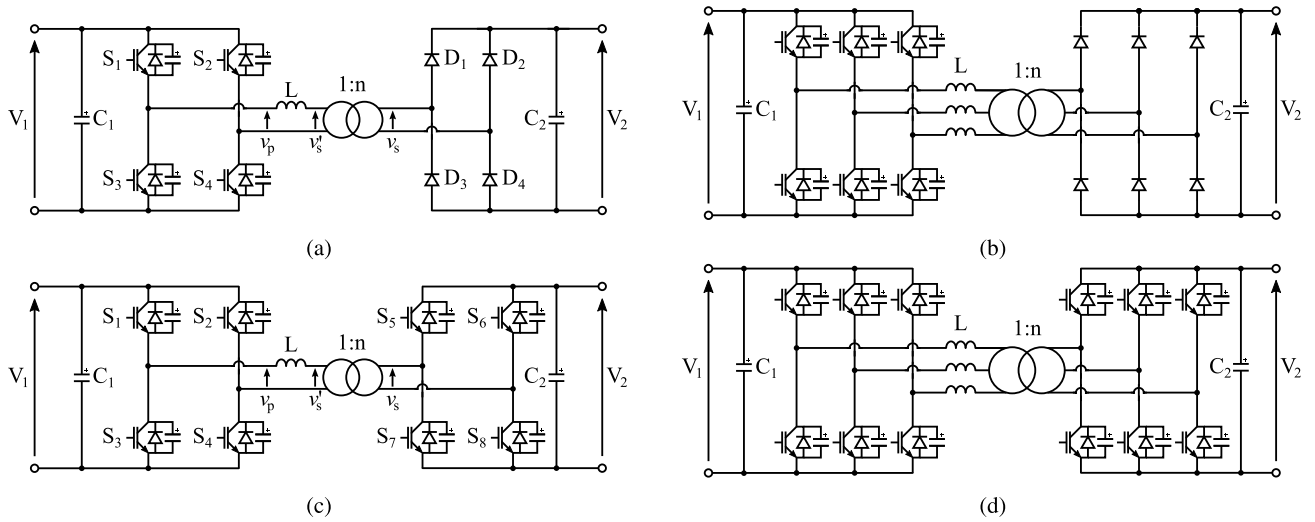

FIGURE 2. Circuit diagrams for the considered DC/DC converter topologies (a) SAB1, (b) SAB3, (c) DAB1, (d) DAB3.

This paper includes a frequency sensitivity study, which details how the selection of the operating frequency can influence the performance and size of the converters. Existing comparison studies typically assume a single converter operating frequency, which can range from as little as 500 Hz [15] up to 10 kHz [19]. This study aims to fill this research gap by providing a quantitative method to select the converter operating frequency.

This study is the first to include an insulation coordination study and to physically arrange the components as part of the volume calculations. This is important because at higher frequencies, the dielectric insulation requirements play an increasingly important role. This is a factor that is currently not addressed in any of existing literature.

Finally, this study examines DC/DC converters fit for modern wind turbines. The rapid development of wind turbines has resulted in assumptions from previous studies to already be outdated. The latest generation of offshore wind turbines are rated at 15 MW. Offshore wind farm array voltages of 66 kV are now standard, with plans for further increases to 132 kV [20]. Wind turbine generator voltages are typically below 1 kV [21], whereas the DC collection system is expected to operate at around ±40 kV (80 kV pole to pole), which is the DC equivalent of 66 kV AC [4]. The DC/DC converter must be designed to be able to handle these high power ratings and large step-up ratios.

The paper is organized as follows: In section II, the four considered topologies and the methodology used in the comparison are set out. In section III, the reliability calculations are performed to determine the required converter redundancy. In section IV, the size and weight of the converter components is calculated, including the transformer, semiconductors and cooling, capacitors, and required isolation clearance. Section V details the efficiency calculation for each of the converters and Section VI sets out the results of the frequency sensitivity studies. Finally, section VII presents the conclusions of the research.

II. TOPOLOGIES AND METHODOLOGY

The converter topologies were selected based on their potential application to the next generation of wind turbines. Four DC/DC converter topologies were investigated and compared for this research. These include the 1-phase single active bridge (SAB1), 3-phase single active bridge (SAB3), 1-phase dual active bridge (DAB1), and 3-phase dual active bridge (DAB3). The circuit diagrams for the topologies are shown in Fig. 2. A detailed description of the converter switching and waveforms under normal operating conditions can be found for each of the converters in [7], [10], [22], and [23]. Despite their potential for high efficiency operation, resonant converter topologies were not included in the analysis, due to their increased complexity and challenges associated with variable frequency operation [24].

There are limited studies which consider converter operation under DC fault conditions. In general, the bidirectional converters have a higher degree of controllability, allowing for more complicated control schemes which can provide fault ride-through capability without overloading the semiconductors [25]. Three-phase converters may also have an advantage over 1-phase converters in fault ride-through capability due to the inherently lower current stresses in the semiconductors.

The methodology used in the converter comparison is illustrated in Fig. 3. The DC/DC converter design starts with the converter availability requirements and device data to calculate the number of redundant modules based on component stresses, failure rates and reliability requirements. For a given operating frequency, the MFT is then designed using a multi-objective optimization, which minimizes the transformer size and losses while meeting the isolation and inductance requirements. PLECS simulations are performed to determine the losses of the semiconductors, as well as to determine the capacitance and heat sink requirements. Once the optimal design is selected, the components are arranged into a minimum volume configuration, taking into account

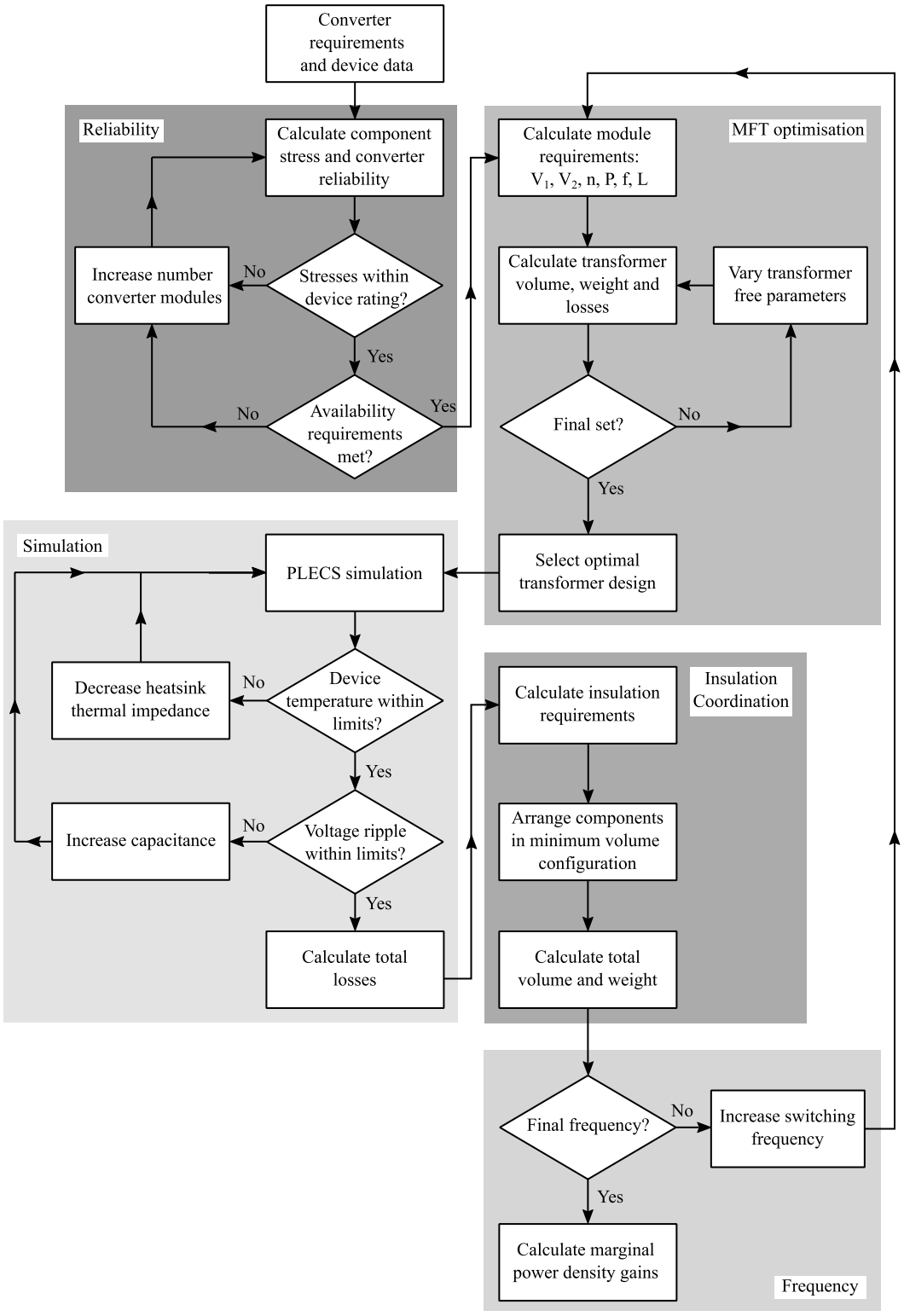

FIGURE 3. Flow diagram outlining the main elements of the methodology used in the converter comparison.

the insulation coordination requirements. The total volume and weight are then calculated for each of the converters. Finally, the frequency is increased and this process is repeated to determine an optimal operating frequency.

III. MODULARITY AND RELIABILITY

A. CONNECTION OPTIONS

The DC/DC converter can either be a standalone design, consisting of a single MFT with series and/or parallel

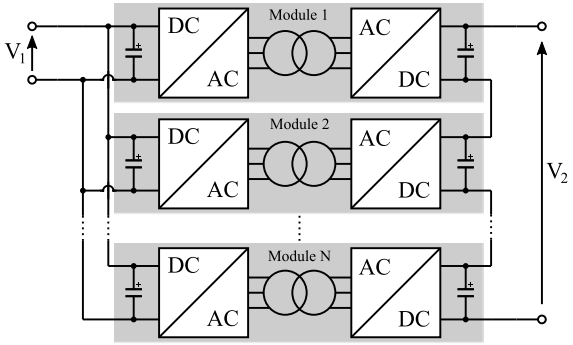

FIGURE 4. Schematic of an input-parallel, output-series cascaded DC/DC converter.

connected switches, or a modular design, which consists of multiple series and/or parallel connected DC/DC converters, each with their own MFT. The standalone or bulk design has the benefit of relatively simple construction. However, modular designs have improved reliability [7] and avoid the need to connect switches in series, which is challenging to implement in practice due to unequal voltage distribution issues [26].

Several options for cascaded connections are possible, including input-series output-series (ISOS), input-series output-parallel (ISOP), input-parallel output-parallel (IPOP), and input-parallel output-series (IPOS) [26]. More complicated arrangements are also possible, including combinations of these connections [27] and the connection of unequally rated converter modules [28], but these were considered beyond the scope of this study.

In general, a series connection results in higher voltage capability, whereas a parallel connection allows for a higher current capability. For the high-power, high voltage step-up requirements of a DC wind turbine, the IPOS connection is most suitable. This topology is illustrated in Fig. 4.

B. MINIMUM NUMBER OF MODULES

The selection of the number of converter modules will have a large impact on the overall converter design and performance metrics. Some papers [29] consider a basic approach where the MFT transformer turns ratio is considered to be 1:1. This has the benefit of reducing the transformer complexity but results in an exceedingly large number of modules required for large voltage step-ups. The inductance required in each module also increases as the total number of modules increases, resulting in a sub-optimal design.

A better approach is to select the number of modules based on semiconductor stresses and converter reliability [30], [31]. The minimum number of modules is determined based on the blocking voltage and current rating of the selected semiconductors, thereby avoiding the series-connection of individual switches, which may be difficult to implement in practice.

The minimum number of series-connected modules required to withstand the voltage can be calculated using

$$k_s = \left\lceil \frac{V_{sw}}{\gamma V_{max}} \right\rceil \tag{1}$$

where V_{sw} is the voltage experienced by the semiconductor, V_{max} is the maximum voltage rating of the semiconductor, and γ is the voltage de-rating factor. The de-rating factor ensures both that there is a safety margin for voltage transients, and that the semiconductor can achieve a reasonable failure-in-time (FIT) [32]. A de-rating factor of 60% is assumed for all semiconductor components.

Similarly, the minimum number of parallel-connected modules required to withstand the current is calculated based on limits given in the datasheet. Semiconductors current limits are typically provided for average current, rms current and repetitive peak current.

$$k_p = \left\lceil \frac{I_{sw}}{I_{max}} \right\rceil \tag{2}$$

where I_{sw} is the average, rms or peak current experienced by the semiconductor and I_{max} is the corresponding maximum current limit provided in the datasheet. Since the number of parallel- and series-connected modules must be equal, the minimum number of modules is given by

$$k = \max(k_s, k_p) \tag{3}$$

C. RELIABILITY

Additional redundant modules can be added to increase the reliability of the converter to an acceptable level for offshore installation, where it is difficult to access and repair turbines located far from shore. The redundant modules can either be on standby until an active module fails, or operate continuously along with the other modules [33]. The second approach is taken here, as it is the industry standard and further reduces the voltage stresses on the semiconductors, thereby reducing their failure rate.

The converter reliability is calculated based on the method used in [31]. The failure rates of individual electrical components are given in Table 1. One converter module consists of the semiconductors of the input and output bridge, the MFT, and the DC capacitors, as shown in the reliability block diagram in Fig. 5. One gate driver was assumed per leg of IGBT switches. The MFT failure rate is assumed to be negligible during the converter lifetime [31]. For the 3-phase topologies, the converter is considered to be operational as long as at least two out of the three legs are healthy, although the maximum power output will be curtailed [22]. A failure of any other component results in the failure of the module.

The base failure rate of the module can be expressed using

$$\lambda_m = \sum N_c \lambda_a \tag{4}$$

where λ_m is the base failure rate of one module, N_c is the number of components, and λ_a is the voltage-adjusted failure rate of each component. The failure rate of semiconductor

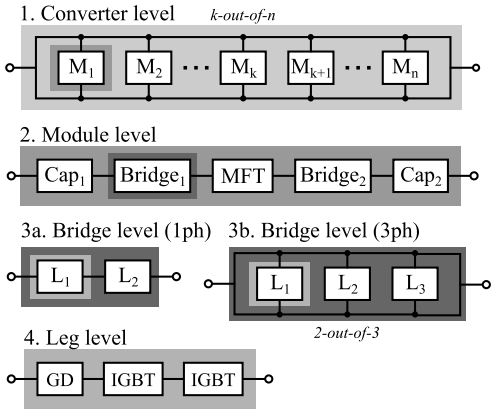

FIGURE 5. Hierarchical reliability block diagram.

TABLE 1. Component annual failure rates and voltage stress factors, based on [31] and [33].

Parameter	Description	Value
λ_{IGBT}	IGBT annual failure rate	0.001752
λ_{GD}	IGBT gate drive annual failure rate	0.004380
λ_D	Diode annual failure rate	0.000438
λ_{cap}	Capacitor annual failure rate	0.000876
η_{IGBT}	IGBT voltage stress factor	2.43
η_D	Diode voltage stress factor	2.43
η_{cap}	Capacitor voltage stress factor	7.5

components and capacitors is exponentially dependent on the applied voltage [33]. The voltage-adjusted failure rates were therefore calculated using the equation

$$\lambda_a = \lambda_c \left(\frac{V_{app}}{V_{nom}} \right)^{\eta} \tag{5}$$

where λ_c is the nominal failure rate of the component, V_{app} is the applied voltage, V_{nom} is the nominal voltage, assumed 60% of V_{max}, and η is the voltage stress factor, given in Table 1. The base availability of one module can then be calculated using

$$A_m = e^{-\lambda_m T_M} \tag{6}$$

where A_m is the base availability of the module and T_M is the preventative maintenance interval.

After obtaining the base availability of one module, the failure rate of the overall converter can then be calculated using the k-out-of-n model, which uses the equation

$$A_c = \sum_{i=k}^{k+R} \frac{(k+R)!}{i!(k+R-i)!} A_m^i (1-A_m)^{(k+R-i)} \tag{7}$$

where k is the minimum number of healthy modules required for converter operation, R is the number of redundant modules and A_m is the availability of one module. Note that the reduction in voltage stresses for higher numbers of redundant modules is taken into account in this calculation.

TABLE 2. Converter and semiconductor parameters.

Parameter	Description	Unit	Value
P_1	Converter input power	MW	15
V_1	Converter input voltage	kV	1.2
V_2	Converter output voltage	kV	80
$V_{IGBT,1}$	Input IGBT voltage rating	kV	1.7
$I_{IGBT,1}$	Input IGBT current rating	kA	1.8
$V_{IGBT,2}$	Output IGBT voltage rating	kV	6.5
$I_{IGBT,2}$	Output IGBT current rating	kA	0.25
$V_{D,2}$	Output diode voltage rating	kV	9.0
$I_{D,2}$	Output diode current rating	kA	0.55
γ	Voltage de-rating factor		60%

TABLE 3. Summary of reliability results for the tested converters.

Converter	Minimum modules	Redundant modules required	Total modules	Availability (%)
SAB1	15	2	17	99.64
SAB3	15	1	16	99.96
DAB1	21	3	24	99.41
DAB3	21	1	22	99.90

D. RESULTS

The system under test considers a 15 MW DC/DC converter with a pole-to-pole output voltage of 80 kV (±40 kV). The input bridge semiconductors were assumed to have a voltage rating of 1.7 kV, which can safely accommodate the wind turbine DC-link voltage with sufficient headroom. The selected IGBT module for the input bridge of all converter topologies is the Infineon FF1800R171P5 [34]. This was selected as it has the highest current rating for an IGBT module for this application. For the output bridge, the highest voltage rating components were selected instead. For the SAB converters, the selected diode is the Infineon D471N [35]. For the output bridge of the DAB converter, the selected IGBT is the Infineon FD250R65KE3-K [36]. The converter and semiconductor parameters are given in Table 2. Based on the semiconductor voltage and current ratings, the minimum number of modules required for the SAB1 and SAB3 was calculated to be 15. For the DAB1 and DAB3, this was calculated to be 21.

Selecting the number of redundant modules presents a trade-off between converter reliability and cost. The target availability and maintenance interval heavily affect the calculations. For this research, a target availability of 99% was selected, with a preventative maintenance interval of one year. Offshore wind turbines typically undergo annual maintenance [37] with continuous condition monitoring allowing for early indication of failure.

The results of the reliability calculations are shown in Fig. 6 and summarized in Table 3. To achieve a 99% probability of failure-free operation in each maintenance interval, the SAB1 converter requires two redundant modules, the DAB1 converter requires three redundant modules, whereas the SAB3 and DAB3 converters both require one redundant module.

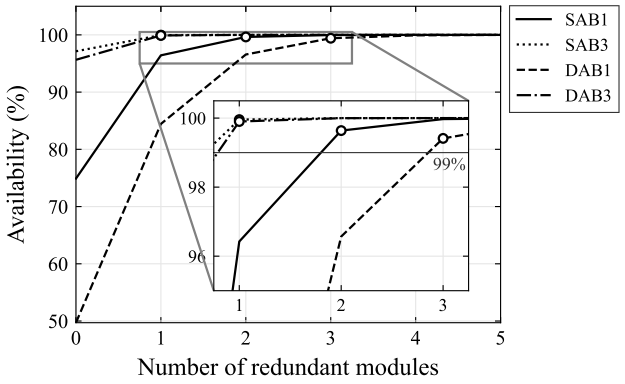

FIGURE 6. Probability of failure-free operation by number of redundant modules. The markers indicate the minimum number of redundant modules for 99% availability.

IV. SIZE AND WEIGHT

The main components of the DC/DC converters are the MFT, the semiconductors and their associated cooling, and the DC-link capacitors. These components have to be housed in an enclosure with the sufficient clearance to fulfil insulation coordination requirements. Each of these elements needs to be assessed to determine the overall weight and volume of the converter.

A. TRANSFORMER

The MFT design is highly dependent on the selected frequency, which is a trade off between weight and efficiency. The size and weight calculations are set out here for a base case frequency of 1 kHz. The results for the other tested frequencies are provided in section VI.

An off-the-shelf transformer cannot be used due to the non-standard frequency, high power and specific leakage inductance requirements. Instead, the MFT must be designed for this application. The transformer design procedure is based on that set out in [38] and [39]. The 1-phase transformers are considered to be shell type with the low and high voltage windings concentrically wound around the central limb. The geometry is illustrated in Fig. 7. In the figure, the subscripts 1 and 2 denote the primary and secondary windings, respectively. The 3-phase transformers are assumed to be core type with the low and high voltage windings wound concentrically around each of the three limbs.

The design procedure starts with the specification of fixed design parameters, such as nominal power, input and output voltages and frequency. In addition, the core and insulation materials are selected, shown in Table 4. The transformer windings are assumed to be copper foil in the primary to accommodate the high currents, and litz wires in the secondary to reduce the inter-winding capacitance [40]. The insulation material is assumed to be CoolPoly-D5108, which is a thermally conductive insulation polymer [38]. Research has shown that the insulation breakdown strength decreases for higher frequency operation [41]. Therefore, the

TABLE 4. Material properties for the MFT [30], [38].

Symbol	Property	Unit	Value
B_{sat}	Core magnetic saturation	T	1.17
ρ_c	Core density	kg/m^3	7330
k_c	Core fill factor		0.75
κ	First Steinmetz constant	W/m^3	0.036
α	Second Steinmetz constant		1.64
β	Third Steinmetz constant		2.10
E_{max}	Max. insulation strength	kV/mm	29

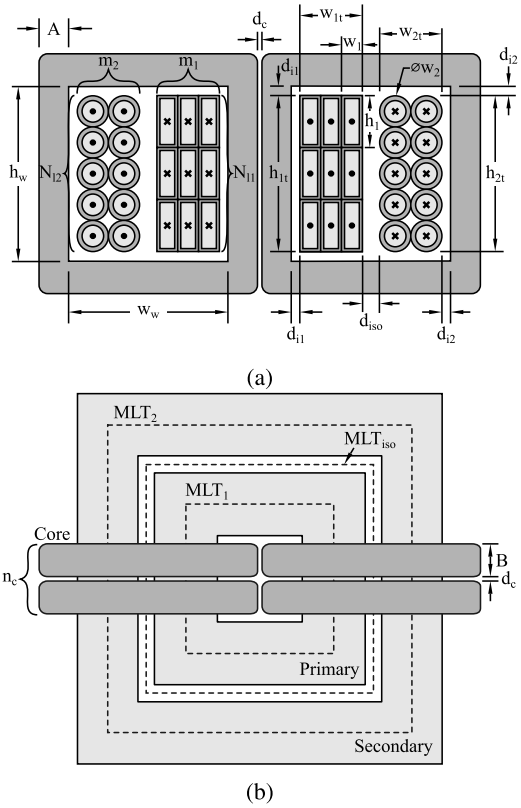

FIGURE 7. Design parameters for the 1-phase medium frequency transformer, (a) front view, (b) top view.

maximum insulation strength was assumed decease linearly from 29 kV/mm at 500 Hz to 24 kV/mm at 5 kHz.

Once the fixed parameters are set, there are a series of free parameters which can be varied to obtain an optimal design. These include the number of parallel layers in the primary and secondary windings (m_1 and m_2), the number of turns per layer in the primary (N_{l1}), the number of core stacks (n_c), the ratio of the limb width to thickness (r_{AB}), and the current density of the primary and secondary windings (J_1 and J_2).

Firstly, the required core cross section is calculated using

$$A_{core} = \frac{\lambda_1}{2N_1 B_{max} k_c} \tag{8}$$

where N_1 is the number of turns in the primary, B_{max} is the maximum flux density, assumed to be 80% of the core material's saturation flux density, k_c is the core fill factor.

The maximum flux linkage, λ_1, is calculated by integrating the positive half cycle of the induced voltage

$$\lambda_1 = \int_0^{T_{pos}} v_p(t)\,dt = \frac{k_\lambda V_1}{f} \tag{9}$$

where k_λ is equal to 0.43 for the SAB1, 0.5 for the DAB1, and 0.22 for the SAB3 and DAB3, provided the duty cycle of the SAB3 is more than $\frac{1}{3}$.

The width A of each limb and yoke is calculated using

$$A = \sqrt{\frac{A_{core} r_{AB}}{2 n_c}} \tag{10}$$

where r_{AB} is the ratio of the limb width to thickness, and n_c is the number of core stacks. Note that the width of the middle limb is $2A$ for the 1-phase transformer. For the 3-phase transformer, all three limbs are of equal width, which is calculated instead using

$$A = \sqrt{\frac{A_{core} r_{AB}}{n_c}} \tag{11}$$

The limb thickness is given by

$$B = \frac{A}{r_{AB}} \tag{12}$$

The insulation distances between the windings and the core are calculated using

$$d_i = \frac{V_{max}}{k_{saf} E_{max}} \tag{13}$$

where V_{max} is the maximum voltage of the winding, assumed to be 1.05 pu of the nominal value, k_{saf} is the safety factor, assumed to be 0.3 [38], and E_{max} is the maximum electric field strength of the insulation material.

The required area of copper in the primary and secondary winding is based on the selected current density,

$$A_{Cu} = \frac{I}{J k_f} \tag{14}$$

where I is the current in the winding, J is the current density of the winding, and k_f is the copper fill factor, which is assumed to be unity for foil and 0.75 for Litz wire [39].

The dimensions of the turns in each winding are calculated based on the copper area. For the Litz wire in the secondary, this can be readily calculated. For the foil, the width is set to the skin depth at the switching frequency [39], allowing the height to be calculated based on the copper area.

$$w_1 = \sqrt{\frac{2\rho_{Cu}}{2\pi f \mu_{Cu}}};\; h_1 = \frac{A_{Cu1}}{w_1};\; w_2 = 2\sqrt{\frac{A_{Cu2}}{\pi}} \tag{15}$$

where ρ_{Cu} is the resistivity of copper, μ_{Cu} is the permeability of copper and f is the switching frequency.

The total height and width of the winding is calculated by multiplying these by the number of layers N_l and number of parallel windings m, respectively.

The required transformer window height is calculated using

$$h_w = \max(h_{1t}, h_{2t}) + 2\,d_i \tag{16}$$

To calculate the transformer window width, the isolation distance d_{iso} between the LV and HV windings must first be calculated. The transformer leakage inductance is used to design the isolation distance. The leakage inductance for a transformer with unequal winding height can be approximated based on an equation from the software ATP Draw [42]

$$L = \mu_0 N_1^2 \left(\frac{MLT_1 w_{1t}}{3h_{1t}} + \frac{MLT_2 w_{2t}}{3h_{2t}} + \frac{2MLT_{iso} d_{iso}}{h_{1t} + h_{2t}} \right) \tag{17}$$

where μ_0 is the permeability of free space and MLT is the mean length of a turn. The mean length of the turns are calculated as follows [38]:

$$MLT_1 = 2\big(2A + 4\,d_{i1} + n_c B + n_c d_c + 2\,w_{1t}\big) \tag{18}$$

$$MLT_{iso} = MLT_1 + 2(4w_{1t} + 2\,d_{iso}) \tag{19}$$

$$MLT_2 = MLT_{iso} + 2\big(2w_{2t} + 2\,d_{iso}\big) \tag{20}$$

where d_c is the distance between the cores, assumed to be 1 mm in both the frontal and lateral directions. Rearranging these equations allows the isolation distance to be calculated.

Finally, the magnetic mean path length for a single transformer core is given as

$$l_m = 2(h_w + A) + 2(w_w + A) \tag{21}$$

resulting in a volume of the transformer core of

$$V_{core} = 2\,n_c l_m AB \tag{22}$$

For the 3-phase transformer, the total magnetic mean path length per core is instead calculated using

$$l_m = 3(h_w + A) + 2(2w_w + 2A) \tag{23}$$

with a transformer core volume of

$$V_{core} = n_c l_m AB \tag{24}$$

The transformer core weight can then be calculated using

$$M_{core} = V_{core} \rho_c. \tag{25}$$

Similarly, the volume and weight of the insulation and copper windings can be calculated using their dimensions and density.

The transformer design results for each of the converters are shown in Fig. 8. The variation of free parameters results in a large space of solutions, for which a Pareto front between efficiency and total mass was calculated. The final design selection was performed by minimising the objective function

$$f_{obj} = \left(\frac{P_{tr}}{P_{tr,min}} \right)^2 + \frac{M_{tot}}{M_{tot,min}} + \frac{V_{tot}}{V_{tot,min}} \tag{26}$$

where P_{tr} are the nominal transformer losses, described in more detail in section V, M_{tot} is the total mass of the

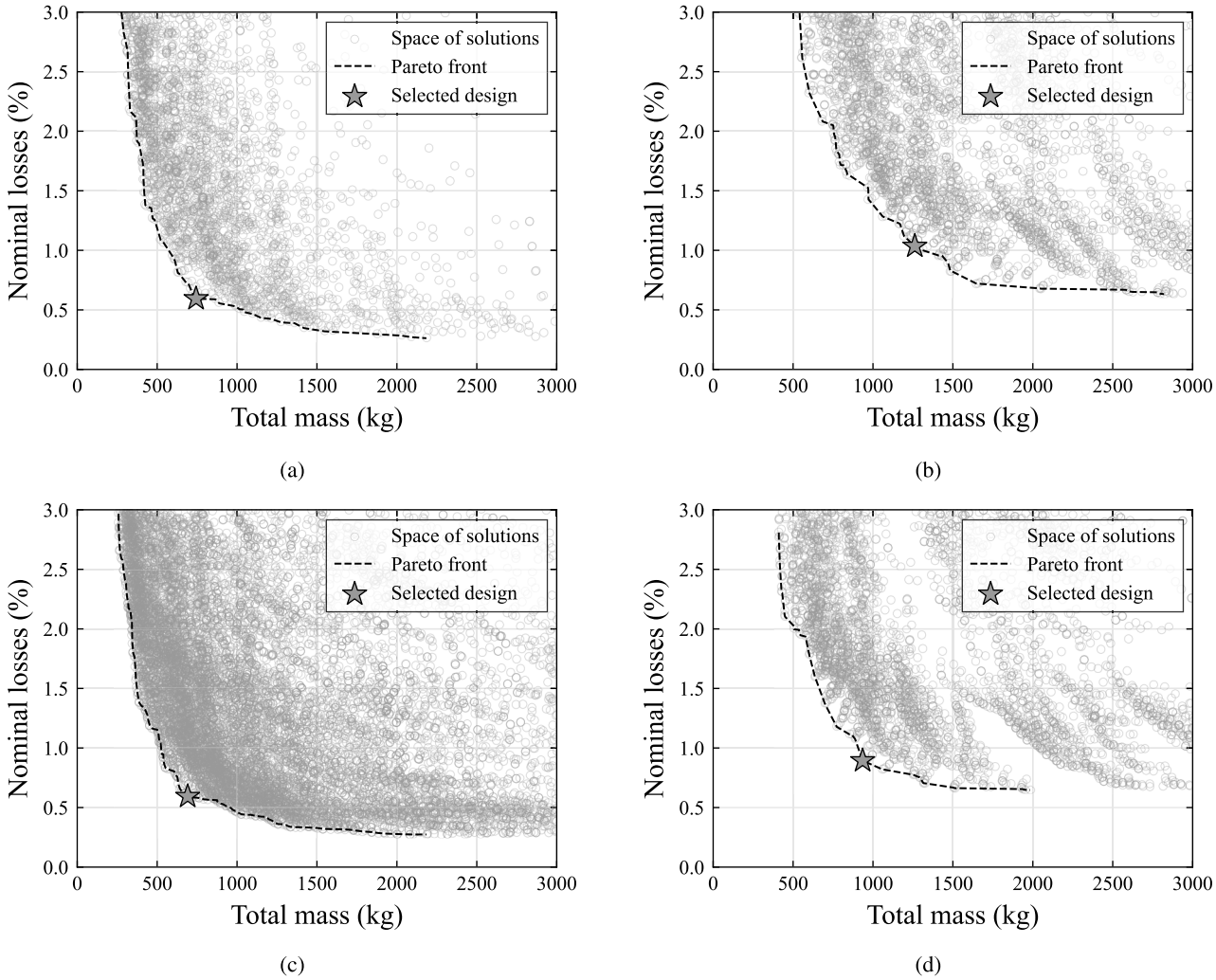

FIGURE 8. Pareto-optimal front for transformer nominal losses against total mass for the tested transformer designs at a base case frequency of 1 kHz, (a) SAB1, (b) SAB3, (c) DAB1, (d) DAB3.

transformer, and V_{tot} is the total volume of the transformer. The subscript min indicates the designs with the lowest value for each of these parameters.

B. SEMICONDUCTORS AND COOLING

Most of the volume and weight associated with semiconductors devices are due to the thermal management system. For high-power applications, such as wind turbine converters, the heat generated by semiconductor losses is typically removed by a water-based cooling system.

The design of a water-based cooling system is beyond the scope of this research. However, existing commercially available components can be used to make a high-level volume and weight estimate. For example, Semikron-Danfoss produce a complete water-cooled 3-phase inverter for wind turbine applications. This system has a mass of 106 kg and volume of 0.125 m^3. It uses a glycol-water mixture resulting in a minimum thermal resistance of 0.006 °C/W [43]. For the 1-phase converters, the input and output bridges consist of two legs instead of three. These were therefore assumed to have two thirds the volume and weight of the 3-phase converters.

Simulations were performed in PLECS to determine the required heatsink resistance to limit the semiconductor junction temperature to 150°C. The semiconductor junction temperature was calculated in PLECS by using the semiconductor transient thermal impedance, obtained from datasheets, combined with the simulated switching and conduction losses. The losses are discussed in further detail in section V. The ambient temperature of the converter was assumed to be 50°C. For the 1 kHz base case, the required thermal resistance of the heatsink to the ambient are given in Table 5. The results show that these are all within the commercial water-cooling capabilities.

C. CAPACITORS

The primary function of the DC link capacitors is to reduce the steady-state input and output voltage ripple. In addition, the capacitance will also influence the controller dynamics and transient converter response to distur-

TABLE 5. Heat sink maximum thermal resistance per module for each converter type for the base case.

Converter	$R_{\theta hs}$ (K/W)	
	Input	Output
SAB1	0.02	10
SAB3	0.037	10
DAB1	0.056	0.052
DAB3	0.09	0.095

TABLE 6. Converter module minimum input and output capacitance for the base case.

Converter	Capacitance (μF)	
	Input	Output
SAB1	7300	310
SAB3	1800	300
DAB1	1300	160
DAB3	340	50

bances [44]. A maximum steady-state voltage ripple of $\pm 1\%$ on the input and output was selected to enable safe generator operation and DC/AC conversion at the grid. The capacitance for each converter module was set to the minimum value which could achieve this voltage ripple while maintaining stable converter operation. The resulting values are given in Table 6.

The volume and weight estimation of the capacitors is based on the approach used in [16]. The capacitor volume is assumed to be proportional to the stored energy and therefore scales linearly with the capacitance, using the equation

$$V_{cap} = k_{c1} C + k_{c0} \tag{27}$$

where C is the capacitance in F, and the parameters k_{c1} and k_{c0} are calculated using linear regression of reference capacitor sizes and voltages. The EPCOS MKP 25680 series capacitors were used as a [45]. The resulting parameters were found to be

$$k_{c1} = 5.22\, U_{cap} - 4.06 \tag{28}$$

$$k_{c0} = 2.181 \times 10^{-4}\, U_{cap} - 6.812 \times 10^{-5} \tag{29}$$

where U_{cap} is the capacitor rated voltage in kV. The weight can then be calculated using

$$M_{cap} = \rho_{cap} V_{cap} \tag{30}$$

where V_{cap} is the capacitor volume and ρ_{cap} is the average density of the capacitor, calculated to be 1063 kg/m^3 from the reference datasheet.

D. INSULATION COORDINATION

The overall volume of the DC/DC converters will be significantly larger than the sum of the individual components due to insulation coordination requirements. The detailed design of the high voltage insulation is beyond the scope of this study. However, a high-level estimate of the required volume can be made based on engineering standards.

There are currently no standards that specifically address high power medium voltage DC/DC converters. However, studies considering DC/DC converter insulation propose using the IEC 61800-5-1 standard [46], [47]. This standard provides clearance distances for electrical drive systems to be able to withstand impulse voltages, temporary overvoltages and the working voltage of the circuit. Equipment is categorized into one of four overvoltage categories (OVCs), depending on how it is connected to the supply mains. For high power DC/DC converters, previous studies have proposed using the OVCII or OVCIII categories [46], [47]. Since this study considers converters housed inside wind turbines, which are typically equipped with overvoltage protection, the less conservative OVCII category was used here.

The main converter components, including the MFT, semiconductors with cooling, and the capacitors, need to be arranged into a minimal volume taking into account these clearance requirements. This results in a variant of the classical 3D bin packing problem, for which there is no straightforward solution [48].

A stacking algorithm was created to arrange the components of each module into a minimum volume configuration. The algorithm uses a brute-force approach to find the lowest volume by combining the components in any order, in any combination of the x-, y-, and z-directions, as well as by flipping each component on all three axes. This results in an exponentially increasing computational burden as more components are added together at once. The algorithm therefore combines a maximum of four components, namely the input bridge and cooling, the output bridge and cooling, the MFT, and the output capacitor. This is illustrated in Fig 9a. The clearance requirements were determined using the operating voltage and IEC standard. For example, for the SAB1, the output voltage of each module is 4.7 kV, resulting in a clearance requirement of 25 mm.

Once the dimensions of an individual module were calculated, a simplified algorithm was used to stack two modules at a time while leaving clearance between each module. Finally, the overall dimensions of the enclosure were calculated by adding a clearance of 173.3 mm to the complete stack to account for the total stack voltage of ± 40 kV. This is illustrated in Fig. 9b.

E. RESULTS

The results of the volume and weight comparison are shown in Fig. 10. The results show that at a frequency of 1 kHz, the transformers and IEC 61800-5-1 insulation clearance contributed approximately equally to the total converter volume, and together account for the majority of the converter volume. In terms of weight, the MFT is the single largest contributor, with both the iron core and the solid epoxy insulation making up most of the overall weight.

The SAB1 has the lowest volume and weight of the four tested converters, at 19 m^3 and 16.4 tonnes, respectively.

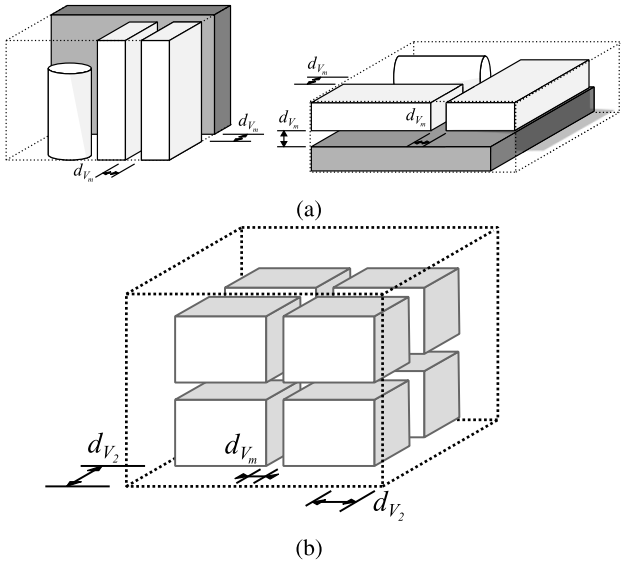

FIGURE 9. Illustration of the stacking algorithm, (a) module-level, (b) converter-level.

This is mainly due to the relatively low number of converter modules. The SAB3 has a volume approximately 61% higher and a weight 45% higher than its 1-phase counterpart, at 30.6 m^3 and 23.7 tonnes, respectively. This is primarily due to the larger 3-phase transformer used in each module.

The selected transformer for the DAB1 is relatively small and light, but the high number of converter modules results in a total volume and weight of 23.4 m^3 and 21.7 tonnes, respectively, which is larger than the unidirectional SAB1. The DAB3, which has a volume of 42.0 m^3 and a weight of 25.3 tonnes, represents an 80% increase in volume and 16% increase in weight, compared to its 1-phase counterpart.

The typical size and weight of a large offshore wind turbine nacelle, such as that of the GE Haliade-X, is 1700 m^3 and 600 tonnes [49]. This means that all of the tested converters are expected to comfortably fit inside the nacelle.

V. EFFICIENCY

The efficiency of each of the four converter topologies was assessed using a combination of simulations and analytical equations. The main loss components considered include the transformer core and winding losses, and the semiconductor switching and conduction losses.

A. TRANSFORMER LOSSES

The transformer copper winding losses are calculated using the methodology based on [39]. The DC winding resistance for each winding is calculated using

$$R_{dc} = \frac{\rho_{Cu} N \text{MLT}}{A_{Cu}} \tag{31}$$

where ρ_{Cu} is the resistivity of copper, and A_{Cu} is the cross-sectional area of the copper.

To account for the skin effect, the ratio of AC to DC resistance at a given harmonic frequency f_h is calculated using the equations

$$K_{ac} = \frac{1}{2} y M_y + (2m-1)^2 D_y \tag{32}$$

where

$$y = \frac{w_c}{\delta};\ \delta = \sqrt{\frac{\rho_{Cu}}{\pi \mu_0 \mu_r f_h}} \tag{33}$$

$$M_y = \frac{\sinh(y) + \sin(y)}{\cosh(y) - \cos(y)} \tag{34}$$

$$D_y = \frac{\sinh(y) - \sin(y)}{\cosh(y) + \cos(y)} \tag{35}$$

where w_c is the conductor width, m is the number of parallel layers in the coil, and μ_r is the relative permeability of copper.

The copper winding losses can then be calculated by summing the losses for each harmonic component

$$P_{Cu} = \sum_h I_h^2 K_{ac,h} R_{dc} \tag{36}$$

where I_h is the magnitude of the current with harmonic order h, and $K_{ac,h}$ is the ratio of AC to DC resistance at the frequency of harmonic order h.

To calculate the iron core losses per unit volume, the Improved Generalized Steinmetz Equation (IGSE) is used. This is defined as [50]

$$P_{core} = \frac{1}{T} \int_0^T k_i \left| \frac{dB}{dt} \right|^\alpha (\acute{}B)^{\beta-\alpha} dt \tag{37}$$

where B is the instantaneous magnetic flux density, $\acute{}B$ is the peak-to-peak magnetic flux density, and k_i is calculated using

$$k_i = \frac{k}{(2\pi)^{\alpha-1} \int_0^{2\pi} |\cos\theta|^\alpha 2^{\beta-\alpha} d\theta} \tag{38}$$

where k, α, and β are the Steinmetz parameters of the iron core material.

B. SEMICONDUCTOR LOSSES

The semiconductor losses consist of the conduction losses and switching losses and were calculated using PLECS. The conduction losses are calculated using

$$P_{cond} = \frac{1}{T} \int_0^T v_{on} i_{on} dt \tag{39}$$

where P_{cond} are the conduction losses, v_{on} is the on-state forward voltage drop of the device, and i_{on} is the current through the device. The on-state voltage drop is determined through linear interpolation of a look-up table, which takes into account the non-linear device resistance and temperature-dependence [51], and is based on the publicly available datasheet [34].

The semiconductor switching losses are calculated using

$$P_{sw} = \frac{1}{T} \sum (E_{on} + E_{off} + E_{rr}) \tag{40}$$

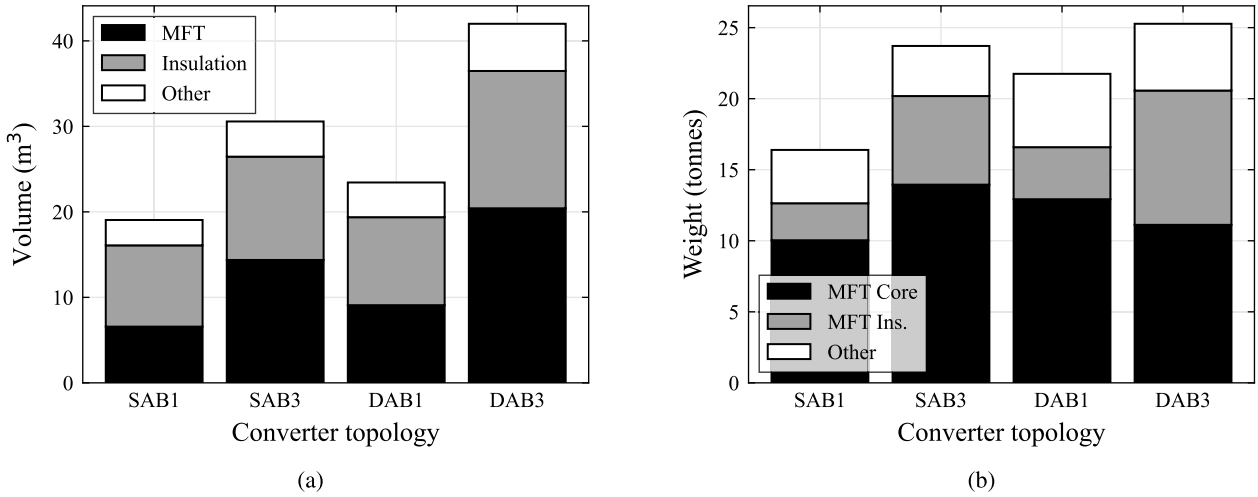

FIGURE 10. Converter stacking results at base case frequency of 1 kHz, (a) volume, and (b) weight.

where E_{on} are the turn-on losses, E_{off} are the turn-off losses and E_{rr} are the reverse recovery losses, which are calculated in PLECS using a 3D lookup table, given by

$$E = f(v_{block}, i_{on}, T) \tag{41}$$

where E is the relevant energy loss during switching, V_{block} is the semiconductor blocking voltage, i_{on} is the on-state current and T is the temperature, all determined either pre- or post-switching [51].

C. RESULTS

The results of the efficiency calculations are shown in Fig. 11. The SAB1 has the lowest losses, ranging from around 1.1% at nominal power to 1.3% at 0.1 pu power output. The main source of losses for this topology are the inverter IGBTs, which experience hard turn-off. The rectifier, on the other hand, has very low losses due to the limited diode conduction losses.

The SAB3 has some of the highest losses at low power output, reaching 2.3% at 0.1 pu. At higher operating points, the converter losses are closer to 1.7%. At lower power outputs, the SAB3 operates in discontinuous current mode, resulting in high turn-off losses for all six inverter IGBTs. In addition, the presence of three phases leads to both higher core and winding losses.

The DAB1 has losses ranging from around 1.5% to 1.9%. The increase compared to the SAB1 is mainly due to the rectifier switching losses. The magnetising voltage for the DAB1 MFT does not change with the operating point, resulting in relatively high transformer core losses at low power outputs.

The DAB3 has similar, albeit slightly higher losses compared to its single phase counterpart, ranging from 1.5% to 2.0%. The additional phases result in higher transformer core and winding losses, which are more significant at lower power outputs. The rectifier losses for the DAB3 are lower than those for the DAB1. This is because the rectifier diodes conduct during more of the switching period, leading in lower currents at IGBT turn-off.

Overall, all four converter topologies have acceptable efficiencies for use in offshore wind turbines. Typical fully rated back-to-back converters used in existing AC-based wind turbines have nominal losses of around 2% [52].

VI. FREQUENCY SENSITIVITY STUDY

The size and efficiency of the converters will be highly dependent on their operating frequency [8]. Therefore, the volume, weight, and losses analysis was repeated for frequencies ranging from 500 Hz to 5 kHz.

In order to use a single measure for the losses at each operating frequency, a representative loss measure was calculated. This was done by weighting the losses at each of the 0.1 pu to 1.0 pu operating points based on the number of hours a generic wind turbine would operate for a given Weibull wind speed distribution. This is explained in more detail in [8].

The results of the frequency sensitivity study are shown in Fig. 12. As expected, an increase in frequency is associated with an increase in losses and a reduction in the volume and weight of the converters. However, the rate of change for each of these factors is different, and they vary by converter topology. In general, the volume reduces more slowly than the mass, expecially at higher frequencies. This is due to the insulation coordination requirements staying the same while the transformer becomes smaller. As a result, the clearance space contributes an increasingly large share to the overall volume. It can also be seen that the volume does not reduce perfectly uniformly as the frequency increases. This is because the MFT design procedure does not take into account stacking efficiency, which means that some MFT dimensions can result in higher overall converter volumes than expected.

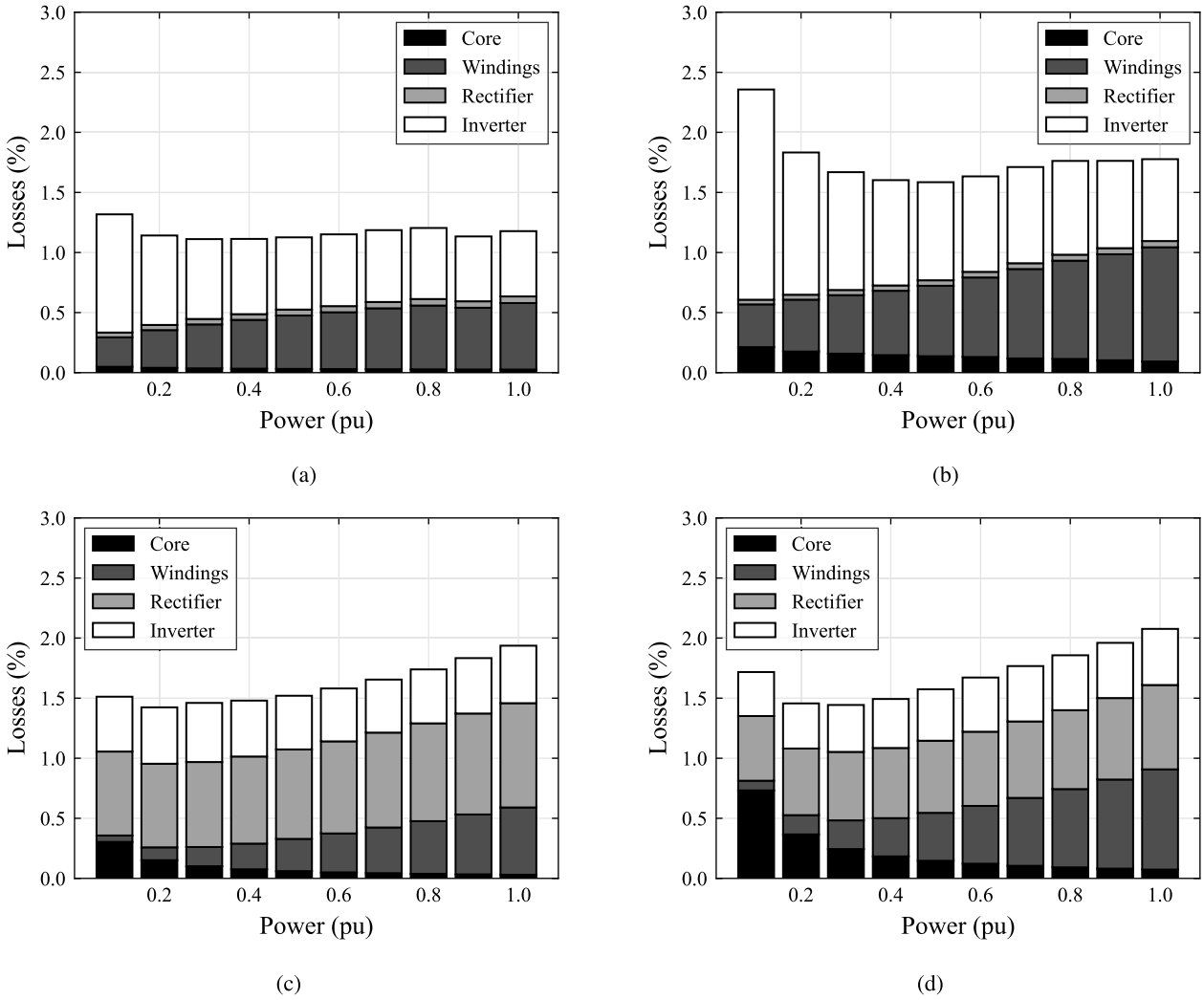

FIGURE 11. Converter losses at base case frequency of 1 kHz, (a) SAB1, (b) SAB3, (c) DAB1, (d) DAB3.

The selection of the optimal frequency will be application-dependent. In this paper, the optimal frequency was selected by taking into account the marginal volumetric and gravimetric power density gains, constrained by the thermal limitations. The volumetric and gravimetric power density gains can be calculated using

$$G_{V_f} = \frac{1 - \frac{V_f}{V_0}}{\frac{P_f}{P_0} - 1}; \quad G_{M_f} = \frac{1 - \frac{M_f}{M_0}}{\frac{P_f}{P_0} - 1} \tag{42}$$

where G_{V_f} and G_{M_f} are the marginal volumetric and gravimetric power density gains at frequency f, V_f, M_f and P_f are the volume, mass and losses at this frequency, and V_0, M_0 and P_0 are the volume, mass and losses of the converter at the lowest frequency. To determine the optimal operating frequency, a minimum value for the marginal power density gains can be selected, depending on the relative importance of each of the factors. In this paper, the minimum required power density gains were set to a value of 2.

Fig. 12a shows that the losses for the SAB1 increase relatively slowly due to the low number of switching devices, from 1.3% at 500 Hz to 2.1% at 5 kHz. Both marginal power density gains are greater than 2 for frequencies up to 2.5 kHz. The high current stress in each device also means that this is the highest switching frequency the commercial water-cooled heatsink can accommodate. For higher frequencies the temperature of the IGBTs would exceed the safe operating range. At a frequency of 2.5 kHz, the losses are still only 1.5%, with a volume and weight reduction of 58% and 75%, respectively, compared to 500 Hz.

It can be seen from Fig. 12b that the losses for the SAB3 increase more rapidly, from 2% to 4% over the tested operating frequency range. The current stresses for the SAB3 are lower, resulting in the cooling being able to manage switching frequencies up to 5 kHz. However, the marginal power density gains are above 2 only for frequencies up to 1.6 kHz. At this frequency, the losses are 2.5%, and the

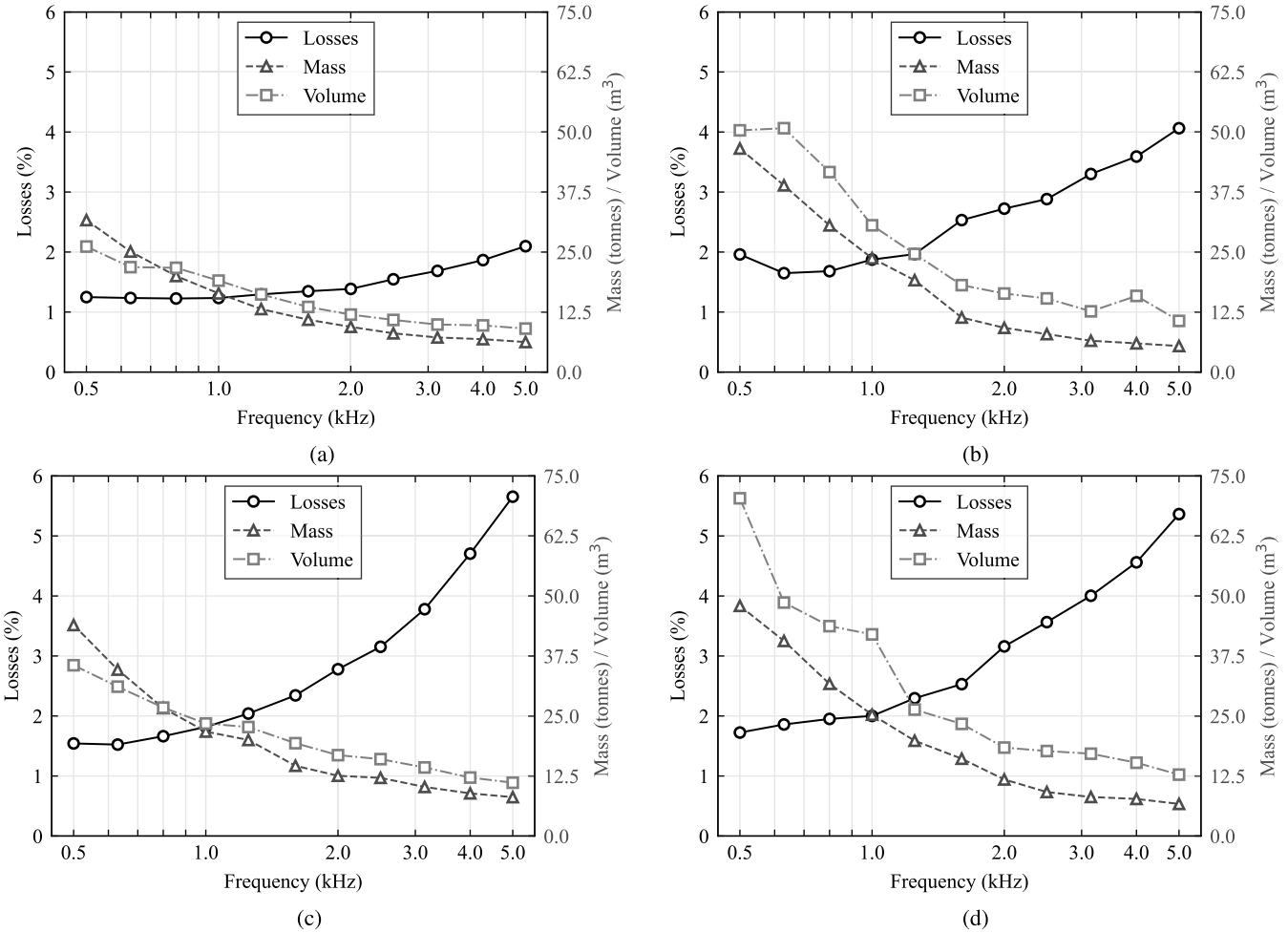

FIGURE 12. Converter losses, volume and mass for operating frequencies ranging from 500 Hz to 5 kHz, (a) SAB1, (b) SAB3, (c) DAB1, (d) DAB3.

volume and mass are 64% and 76% lower than at 500 Hz, respectively.

The results for the DAB1 and DAB3 are shown in Fig. 12c and Fig. 12d, respectively. The losses for both topologies are similar, and increase much more rapidly with frequency than for the unidirectional converters. This is due to the additional switches in the output bridge. The losses for the DAB1 and DAB3 range from approximately 1.5% at 500 Hz to 5.5% at 5 kHz. The DAB1 reaches its thermal limit at a switching frequency of 2.5 kHz, whereas the lower losses per device for the DAB3 mean the converter can operate at switching frequencies up to 4 kHz. However, the marginal power density gains for both converters drops off very quickly, reaching less than 2 at frequencies above 1 kHz. At this frequency, the DAB1 has losses of 1.8%, with a reduction in the volume and weight of of 34% and 50% compared to 500 Hz, respectively. For the DAB3, the values are 2% losses, 40% volume reduction, and 47% weight reduction.

VII. CONCLUSION

This research has presented the optimization and comparison of four cascaded DC/DC converter topologies for a DC-connected offshore wind turbine, including the SAB1, SAB3, DAB1, and DAB3. For each converter, the reliability, size, weight, and losses were calculated at frequencies ranging from 500 Hz to 5 kHz. The MFT was designed by employing a multi-objective optimization procedure, aimed at minimizing the transformer size, weight, and losses. The overall converter volume was calculated using a stacking algorithm to minimize the volume while accounting for the IEC 61800-5-1 clearance requirements. The optimal frequency was selected by calculating the marginal gains in power density.

The SAB1 is a 1-phase unidirectional converter which uses diodes in the rectifier. It requires 17 IPOS connected modules to achieve an availability of 99%. The SAB1 can operate at a relatively high frequency of 2.5 kHz, making it the smallest, lightest, and most efficient of the tested converters. At this frequency, it has a volume of 10.9 m^3, a weight of 8.0 tonnes, and representative losses of 1.5%.

The SAB3 is the 3-phase equivalent of the SAB1. It requires a total of 16 IPOS connected modules to achieve 99% availability, which is the lowest of all tested converters. However, its optimal operating frequency is 1.6 kHz, and it has a higher volume, higher weight and higher losses than its 1-phase counterpart, at 18.1 m^3, 11.4 tonnes, and 2.5%,

respectively. If only unidirectional power is needed, the SAB1 is therefore preferred over the SAB3.

The bidirectional DAB1 and DAB3 converters use IGBTs in both the inverter and rectifier. The lower voltage ratings and higher failure rate of these switches compared to diodes results in a larger number of IPOS connected modules required. The DAB1 and DAB3 require a total of 24 and 22 IPOS connected modules, respectively. The DAB1 and DAB3 both have an optimal operating frequency of 1 kHz due to the rapid increase in losses for higher frequencies. At 1 kHz, the DAB1 has losses of 1.8%, a volume of 23.4 m^3, and a weight of 21.7 tonnes. The DAB3 has slightly higher losses of 2%, but is significantly larger at 42.0 m^3 and 25.2 tonnes. If bidirectional power is needed, and there are no space concerns, the DAB3 is the preferred topology due to its higher reliability and lower device stresses.

REFERENCES

[1] *Energy Transition Outlook 2022—A Global and Regional Forecast to 2050*, 2022.
[2] TenneT. (2024). *The 2 GW Program*. Accessed: Feb. 8, 2024.
[3] (2024). *V236-15mw*. Accessed: Feb. 8, 2024. [Online]. Available: https://www.vestas.com/en/energy-solutions/offshore-wind-turbines/V236-15MW
[4] V. Timmers, A. Egea-Àlvarez, A. Gkountaras, R. Li, and L. Xu, "All-DC offshore wind farms: When are they more cost-effective than AC designs?" *IET Renew. Power Gener.*, vol. 17, no. 10, pp. 2458–2470, Jul. 2023.
[5] *Offshore Wind Accelerator—-DC Array System Refresh Study*, OWA Rep. 2018, 2018.
[6] M. De Prada Gil, J. L. Domínguez-García, F. Díaz-González, M. Aragüés-Peñalba, and O. Gomis-Bellmunt, "Feasibility analysis of offshore wind power plants with DC collection grid," *Renew. Energy*, vol. 78, pp. 467–477, Jun. 2015.
[7] V. Timmers, A. Egea-Àlvarez, A. Gkountaras, and L. Xu, "Review and comparison of single and dual active bridge converters for MVDC-connected wind turbines," in *Proc. 21st Wind Sol. Integr. Workshop (WIW)*, vol. 2022, Oct. 2022, pp. 509–516.
[8] V. Timmers, A. Egea-Àlvarez, and A. Gkountaras, "Frequency optimisation for DC/DC converters in DC-connected offshore wind turbines," in *Proc. 25th Eur. Conf. Power Electron. Appl.*, Sep. 2023, pp. 1–8.
[9] L. Max and S. Lundberg, "System efficiency of a DC/DC converter-based wind farm," *Wind Energy*, vol. 11, no. 1, pp. 109–120, Jan. 2008.
[10] K. Park and Z. Chen, "Analysis and design of a parallel-connected single active bridge DC–DC converter for high-power wind farm applications," in *Proc. 15th Eur. Conf. Power Electron. Appl. (EPE)*, Sep. 2013, pp. 1–10.
[11] S. P. Engel, N. Soltau, H. Stagge, and R. W. De Doncker, "Dynamic and balanced control of three-phase high-power dual-active bridge DC–DC converters in DC-grid applications," *IEEE Trans. Power Electron.*, vol. 28, no. 4, pp. 1880–1889, Apr. 2013.
[12] W. Chen, A. Q. Huang, C. Li, G. Wang, and W. Gu, "Analysis and comparison of medium voltage high power DC/DC converters for offshore wind energy systems," *IEEE Trans. Power Electron.*, vol. 28, no. 4, pp. 2014–2023, Apr. 2013.
[13] D. Jovcic, "Step-up DC–DC converter for megawatt size applications," *IET Power Electron.*, vol. 2, no. 6, pp. 675–685, Nov. 2009.
[14] A. Parastar and J.-K. Seok, "High-gain resonant switched-capacitor cell-based DC/DC converter for offshore wind energy systems," *IEEE Trans. Power Electron.*, vol. 30, no. 2, pp. 644–656, Feb. 2015.
[15] Y. Zhou, D. E. Macpherson, W. Blewitt, and D. Jovcic, "Comparison of DC–DC converter topologies for offshore wind-farm application," in *Proc. 6th IET Int. Conf. Power Electron., Mach. Drives*, Mar. 2012, pp. 1–6.
[16] R. Barrera-Cardenas and M. Molinas, "Comparative study of wind turbine power converters based on medium-frequency AC-link for offshore DC-grids," *IEEE J. Emerg. Sel. Topics Power Electron.*, vol. 3, no. 2, pp. 525–541, Jun. 2015.
[17] T. Jimichi, M. Kaymak, and Rik. W. De Doncker, "Comparison of single-phase and three-phase dual-active bridge DC–DC converters with various semiconductor devices for offshore wind turbines," in *Proc. IEEE 3rd Int. Future Energy Electron. Conf. ECCE Asia*, Jun. 2017, pp. 591–596.
[18] W. Chen, G. Wang, and X. Zhu, "A family of bidirectional DC/DC converters suitable for asymmetrical power flow requirement," in *Proc. IEEE Energy Convers. Congr. Expo.*, Sep. 2013, pp. 4878–4881.
[19] T. Lagier and P. Ladoux, "A comparison of insulated DC–DC converters for HVDC off-shore wind farms," in *Proc. Int. Conf. Clean Electr. Power (ICCEP)*, Jun. 2015, pp. 33–39.
[20] *Unlocking the Next Generation of Offshore Wind: Step Change To 132kV Array Systems*, 2022.
[21] W. Chen, A. Huang, S. Lukic, J. Svensson, J. Li, and Z. Wang, "A comparison of medium voltage high power DC/DC converters with high step-up conversion ratio for offshore wind energy systems," in *Proc. IEEE Energy Convers. Congr. Exposit.*, Sep. 2011, pp. 584–589.
[22] Y. Sang, A. Junyent-Ferré, and T. C. Green, "Operational principles of three-phase single active bridge DC/DC converters under duty cycle control," *IEEE Trans. Power Electron.*, vol. 35, no. 8, pp. 8737–8750, Aug. 2020.
[23] R. W. A. A. De Doncker, D. M. Divan, and M. H. Kheraluwala, "A three-phase soft-switched high-power-density DC/DC converter for high-power applications," *IEEE Trans. Ind. Appl.*, vol. 27, no. 1, pp. 63–73, Jul. 1991.
[24] Y. Wei, Q. Luo, and H. A. Mantooth, "LLC and CLLC resonant converters based DC transformers (DCXs): Characteristics, issues, and solutions," *CPSS Trans. Power Electron. Appl.*, vol. 6, no. 4, pp. 332–348, Dec. 2021.
[25] J. Hu, S. Cui, and R. W. De Doncker, "DC fault ride-through of a three-phase dual-active bridge converter for DC grids," in *Proc. Int. Power Electron. Conf.*, May 2018, pp. 2250–2256.
[26] Y. Lian, "DC/DC converter for offshore DC collection network," Ph.D. thesis, Dept. Electron. Elect. Eng., Univ. Strathclyde, Glasgow, U.K., 2016.
[27] Y. Lian, G. P. Adam, D. Holliday, and S. J. Finney, "Medium-voltage DC/DC converter for offshore wind collection grid," *IET Renew. Power Gener.*, vol. 10, no. 5, pp. 651–660, May 2016.
[28] K. Park and Z. Chen, "A double uneven power converter-based DC–DC converter for high-power DC grid systems," *IEEE Trans. Ind. Electron.*, vol. 62, no. 12, pp. 7599–7608, Dec. 2015.
[29] M. Kaymak, R. W. De Doncker, and T. Jimichi, "Design and verification of a medium-frequency transformer in a three-phase dual-active bridge DC–DC converter for medium-voltage grid connection of offshore wind farms," in *Proc. IEEE Appl. Power Electron. Conf. Expo.*, Mar. 2020, pp. 2694–2701.
[30] M. Mogorovic and D. Dujic, "Sensitivity analysis of medium-frequency transformer designs for solid-state transformers," *IEEE Trans. Power Electron.*, vol. 34, no. 9, pp. 8356–8367, Sep. 2019.
[31] G. Abeynayake, G. Li, T. Joseph, J. Liang, and W. Ming, "Reliability and cost-oriented analysis, comparison and selection of multi-level MVdc converters," *IEEE Trans. Power Del.*, vol. 36, no. 6, pp. 3945–3955, Dec. 2021.
[32] M. Stieneker and R. W. De Doncker, "Dual-active bridge DC–DC converter systems for medium-voltage DC distribution grids," in *Proc. IEEE 13th Brazilian Power Electron. Conf. 1st Southern Power Electron. Conf. (COBEP/SPEC)*, Brazil, Nov. 2015, pp. 1–6.
[33] J. Guo, X. Wang, J. Liang, H. Pang, and J. Gonçalves, "Reliability modeling and evaluation of MMCs under different redundancy schemes," *IEEE Trans. Power Del.*, vol. 33, no. 5, pp. 2087–2096, Oct. 2018.
[34] Infineon Technol. AG. (2020). *Datasheet FF1800R17IP5*. [Online]. Available: https://www.infineon.com/cms/en/product/power/igbt/igbt-modules/ff1800r17ip5/
[35] Infineon Technol. AG. (2014). *Datasheet D471N*. [Online]. Available: https://www.infineon.com/cms/en/product/power/diodes-thyristors/thyristor-diode-discs/diode-discs/rectifier-diodes/d471n90t/
[36] Infineon Technol. AG. (2021). *Datasheet FD250R65KE3-K*. [Online]. Available: https://www.infineon.com/cms/en/product/power/igbt/igbt-modules/fd250r65ke3-k/
[37] *Outline Offshore Operations and Maintenance Plan*, document DCO 8.11, 2018.
[38] M. A. Bahmani, T. Thiringer, and M. Kharezy, "Design methodology and optimization of a medium-frequency transformer for high-power DC–DC applications," *IEEE Trans. Ind. Appl.*, vol. 52, no. 5, pp. 4225–4233, Sep. 2016.
[39] L. Max, "Energy Eval. for DC/DC converters in DC-based wind farms," Ph.D. thesis, Dept. Energy Environ., Chalmers Univ. Technol., Gothenburg, Sweden, 2007.
[40] M. Bahmani, "Design optim. Considerations medium-frequency power transformers high-power DC–DC applications," Ph.D. thesis, Dept. Energy Environ., Chalmers Univ. Technol., Gothenburg, Sweden, 2016.

[41] W. Wang, X. Wang, J. He, Y. Liu, S. Li, and Y. Nie, "Electric stress and dielectric breakdown characteristics under high-frequency voltages with multi-harmonics in a solid-state transformer," *Int. J. Electr. Power Energy Syst.*, vol. 129, Jul. 2021, Art. no. 106861.
[42] M. Lambert, F. Sirois, M. Martinez-Duro, and J. Mahseredjian, "Analytical calculation of leakage inductance for low-frequency transformer modeling," *IEEE Trans. Power Del.*, vol. 28, no. 1, pp. 507–515, Jan. 2013.
[43] *SEMISTACK Renewable Energy—Size W2*, document SKS B2 140 GD 69/12 U, Semikron-Danfoss, 2013.
[44] K. Park and Z. Chen, "Control and dynamic analysis of a parallel-connected single active bridge DC–DC converter for DC-grid wind farm application," *IET Power Electron.*, vol. 8, no. 5, pp. 665–671, May 2015.
[45] (2022). *Film Capacitors—Power Electronic Capacitors*. [Online]. Available: https://www.tdk-electronics.tdk.com/inf/20/50/ds/mkp_dc_b2568x.pdf
[46] A. Christe, E. Coulinge, and D. Dujic, "Insulation coordination for a modular multilevel converter prototype," in *Proc. 18th Eur. Conf. Power Electron. Appl.*, Sep. 2016, pp. 1–9.
[47] S. Ozdemir, N. Altin, A. Nasiri, and R. Cuzner, "Review of standards on insulation coordination for medium voltage power converters," *IEEE Open J. Power Electron.*, vol. 2, pp. 236–249, Mar. 2021.
[48] S. Martello, D. Pisinger, and D. Vigo, "The three-dimensional bin packing problem," *Oper. Res.*, vol. 48, no. 2, pp. 256–267, Apr. 2000.
[49] Z. Jiang, "Installation of offshore wind turbines: A technical review," *Renew. Sustain. Energy Rev.*, vol. 139, Apr. 2021, Art. no. 110576.
[50] K. Venkatachalam, C. R. Sullivan, T. Abdallah, and H. Tacca, "Accurate prediction of ferrite core loss with nonsinusoidal waveforms using only steinmetz parameters," in *Proc. IEEE Workshop Comput. Power Electron.*, Apr. 2002, pp. 36–41.
[51] Plexim GmbH. (2022). *PLECS User Manual Version 4.6*. [Online]. Available: https://www.plexim.com/sites/default/files/plecsmanual.pdf
[52] (2024). *Technical Data PCS6000 Medium Voltage Wind Turbine Converter*. Accessed: Mar. 5, 2024. [Online]. Available: https://new.abb.com/power-converters-inverters/wind-turbines/utility-scale/pcs6000/technical-data

VICTOR TIMMERS received the B.Eng. (Hons.) and M.Sc. degrees from The University of Edinburgh, U.K., in 2017 and 2018, respectively. He is currently pursuing the Ph.D. degree in electronic and electrical engineering with the University of Strathclyde. He worked for two years as a Power Systems Engineer with Mott MacDonald. His research interests include converter control and optimization, electrolyser integration, and dc collection systems for offshore wind.

AGUSTÍ EGEA-ÀLVAREZ (Member, IEEE) received the B.Sc., M.Sc., and Ph.D. degrees from the Technical University of Catalonia, Barcelona, in 2008, 2010, and 2014, respectively. In 2015, he was a Marie Curie Fellow with China Electric Power Research Institute (CEPRI). In 2016, he joined Siemens Gamesa Renewable Energy as a Converter Control Engineer, working on grid-forming controllers and alternative HVDC schemes for offshore wind farms. He is currently a Reader with the Electronic and Electrical Engineering Department and a member with the Power Electronics, Drives and Energy Conversion (PEDEC) Group. Also, he is the Holder of the Royal Academy of Engineering Industrial Fellowship, ScottishPower. He is a member of IET and has been involved in several CIGRE working groups.

ARIS GKOUNTARAS received the Diploma degree in electrical and computer engineering from AUTH, Greece, in 2011, and the Ph.D. degree in electrical engineering from TU Berlin, Germany, in 2016. Since 2015, he has been active in the wind industry, dealing with power electronics and grid integration topics. He joined Siemens Gamesa Renewable Energy, in 2020, where he currently holds the position of a Senior Key Expert in electricals and grid integration.

LIE XU (Senior Member, IEEE) received the B.Sc. degree in mechatronics from Zhejiang University, Hangzhou, China, in 1993, and the Ph.D. degree in electrical engineering from The University of Sheffield, Sheffield, U.K., in 2000. He was with the Queen's University Belfast and ALSTOM T&D, Stafford, U.K. He is currently a Professor with the Department of Electronic and Electrical Engineering, University of Strathclyde, Glasgow, U.K. His research interests include power electronics, wind energy generation and grid integration, and the application of power electronics to power systems, such as HVDC and MVDC systems for power transmission and distribution.